Pressure-broadening coefficients and line strengths of H_2O near 1.39 μm: application to the in situ sensing of the middle atmosphere with balloonborne diode lasers

G. Durry[a,b], V. Zeninari[a,*], B. Parvitte[a], T. Le barbu[a,b], F. Lefevre[b], J. Ovarlez[c], R.R. Gamache[d]

[a]*Groupe de Spectrométrie Moléculaire et Atmosphérique, UMR CNRS 6089, UFR Sciences Exactes et Naturelles, Moulin de la Housse, BP 1039, 51687 Reims, Cedex 2, France*
[b]*Service d'Aéronomie du CNRS, CNRS-Réduit de Verrières, BP 3, 91371 Verrières-le-Buisson Cedex, France*
[c]*Laboratoire de Météorologie Dynamique, UMR 8539, Ecole Polytechnique, 91128 Palaiseau, Cedex, France*
[d]*Department of Environmental, Earth, and Atmospheric Sciences, University of Massachusetts Lowell, 265 Riverside Street, Lowell, MA 01854-5045, USA*

Abstract

Since 1998, we have developed two balloonborne diode laser spectrometers, SDLA and micro-SDLA, to yield in situ concentration data of H_2O in the middle atmosphere by absorption spectroscopy in the 1.39-μm spectral range. In this paper, we revisit the molecular parameters, line intensities and pressure-broadening coefficients, for several lines of the $v_1 + v_3$ and $2v_1$ bands, which are useful for the monitoring of atmospheric H_2O. The new values are thoroughly compared to existing molecular database and previous determinations. Calculations are performed to yield the pressure-effect coefficients: the theoretical model is described and the ab initio predictions are compared to laboratory measurements achieved with a laser diode spectrometer. The improvement in the H_2O monitoring obtained with the new set of molecular data is evaluated directly from vertical H_2O concentration profiles.
© 2004 Elsevier Ltd. All rights reserved.

Keywords: Diode laser; Near-infrared spectrometer; Ab initio calculations; Water vapor; Atmospheric applications

*Corresponding author. Tel.: +33 3 26 91 34 45; fax: +33 3 26 91 31 47.
E-mail address: virginie.zeninari@univ-reims.fr (V. Zeninari).

1. Introduction

Since 1998, two balloonborne laser diodes, SDLA and micro-SDLA, have been developed with the support of the French space agency to measure in situ water vapor, methane and carbon dioxide in the lower stratosphere [1]. Both sensors have been involved in several European campaigns to study stratospheric ozone (THESEO in 1999–2000) or to investigate the processes controlling H_2O in tropical regions (HIBISCUS in 2003–2004). Furthermore, the sensors are currently participating to the validation of environmental satellites like GOMOS-H_2O (onboard ENVISAT) and ODIN. The H_2O molecule plays a major role in the radiative and chemical equilibrium of the lower stratosphere, the region of the atmosphere where the ozone layer is found. The observed increase of 1% year in the H_2O content of the lower stratosphere, with suspected impact on the global ozone recovery, is a strong impetus to develop new technique for the in situ monitoring of H_2O. Water vapor is difficult to measure in situ because there are large amounts of water vapor in the lower layers of the Earth atmosphere (20,000 ppmv at ground levels in tropical regions) while the stratosphere is comparatively strongly dehydrated (4–5 ppmv). Diode laser spectroscopy is a powerful sensing method to address the monitoring of H_2O: by combining direct/differential detection technique with an appropriate selection of the H_2O molecular transitions scanned over by the laser, it is possible to achieve a dynamic range of five orders of magnitude for the concentration measurements and therefore to probe continuously H_2O in the middle atmosphere [2]. During the ascent/descent of the balloon gondola in the lower layers of the atmosphere, the laser scans weak H_2O transitions to probe the large amounts of water vapor and direct detection is used to record the spectra, whereas strong transitions are selected in conjunction with differential detection to monitor the dehydrated stratosphere. Purposely, we have had developed by THALES–LCR a dedicated telecommunication-type distributed-feedback InGaAs laser diode emitting from 7165 to 7185 cm^{-1}. That particular spectral domain features essentially H_2O transitions from the $v_1 + v_3$ and $2v_1$ bands, with line intensities ranging from 10^{-20} to 10^{-23} cm^{-1} mol^{-1} cm^2. The laser diode is connected by means of an optical fiber to a multipass cell operated open to the atmosphere, which provides an absorption path of ~50 m. The laser beam is absorbed in situ by the ambient H_2O molecules while it is bouncing back and forth between both mirrors of the cell. In situ absorption spectra are recorded within 1 s at cell output using direct-differential detection technique [1]. Simultaneously, in situ measurement of atmospheric pressure and temperature are taken from dedicated sensor onboard the balloon gondola. The molecular concentration is retrieved from the in situ spectra by applying a non-linear least-squares fit to the full molecular line shape using the corresponding P and T data and an appropriate molecular model. A complete description of concentration retrieval principal and achieved inaccuracy that lays between 5% and 10%, are found in Ref. [1]. The molecular parameters (line strengths and pressure-broadening coefficients) used to relate the absorption of laser energy to the molecular densities are an important source of error; for instance, with the assumption of a weak absorption, the molecular absorption is directly proportional to the line strength. In a previous work, we have observed discrepancies with the HITRAN database in terms of positions and intensities, for several lines reached by the THALES laser [3]. In this paper, we investigate experimentally and theoretically essentially the intensities and pressure-broadening coefficients which are used by the balloonborne laser hygrometer SDLA and micro-SDLA. The effect of error in the intensity and broadening parameter as well as the choice of a Voigt or

Table 1
List of the lines investigated in this work

Line number	Transition $(J_{K_aK_c})$upper $\leftarrow (J_{K_aK_c})$lower	Band	σ_0 (cm^{-1}) [5]	E_0 (cm^{-1}) [5]	γ_{Self} [4] (cm^{-1} atm^{-1})	Altitude range (km)
1	$6_{6\ 0} \leftarrow 6_{6\ 1}$	$\nu_1 + \nu_3$	7185.59600	1045.0588	0.2140	5–8
2	$2_{1\ 2} \leftarrow 3_{1\ 3}$	$\nu_1 + \nu_3$	7182.94955	142.2785	0.4880	8–14
3	$2_{0\ 2} \leftarrow 3_{0\ 3}$	$\nu_1 + \nu_3$	7181.15570	136.7616	0.4630	>14
4	$3_{0\ 3} \leftarrow 3_{2\ 2}$	$\nu_1 + \nu_3$	7175.98675	206.3015	0.4661	<5

Rautian profile to model line shape at atmospheric pressures will be evaluated from in situ vertical concentration profiles of H_2O yielded by the balloonborne instruments.

The list of the lines investigated in this work is presented in Table 1. In the 1.39-μm spectral range, a former study has shown many differences between experimental and calculated spectra using the HITRAN database [4]. Indeed our experimental spectra were in better agreement with those calculated from the data of Toth [5]. Although our frequency calibration is only relative due to the lack of standards, discrepancies with HITRAN positions were observed [3,6]. Therefore the Toth positions were used in our study. The lower energy levels given in Table 1 are also from Toth and are found in agreement with those from HITRAN and from a former study [7]. The self-broadening coefficient γ_{self} given in Table 1 were not determined in this study and the HITRAN value was used. The lines are indicated with the corresponding altitude range where they are usually used for atmospheric retrievals by the SDLA spectrometer.

2. Experimental measurements

2.1. Experimental details

The H_2O spectra are recorded at high resolution in the laboratory with a tunable diode laser (TDL) spectrometer. Our experimental arrangement is schematically shown in Fig. 1.

The laser source is a fiber-coupled distributed feedback (DFB) InGaAs diode laser that has been developed for the SDLA experiment by THALES—France. It exhibits high performance: the average output power is 10 mW, the laser linewidth <10 MHz and there are no mode-hops in the tunability range. The continuous tuning range (at constant temperature) is >3 cm^{-1}. This point is of particular interest for our experiments where the maximum pressure may be 1330 mbar and the collisional line broadening is important. The diode includes a Faraday optical isolator to prevent optical feedback and emits at 7180 cm^{-1} at room temperature with a maximum power of 12 mW while the temperature and current tuning rates are, respectively, 0.09 nm °C^{-1} and 0.0078 nm mA^{-1}. The laser wavelength is temperature stabilized by means of a Peltier element and is driven by a low noise current supply. A low-frequency ramp at 100 Hz is used to scan the DFB diode over the selected absorption lines by modulation of the driving current. The pigtailed laser diode mounted in an emission module is junctioned to a 50/50 fused coupler. The main beam (A) is collimated and passed through an absorption White type cell. The remaining part of the beam is junctioned to a second 50/50 fused coupler. One beam is collimated and coupled with a confocal
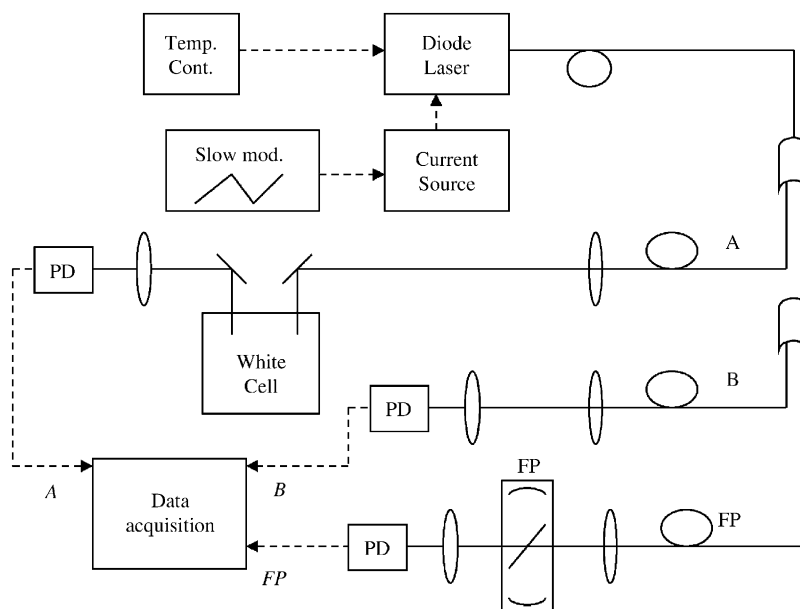
Fig. 1. Scheme of the absorption spectrometer. Temp. Cont. stands for temperature controller, Slow mod. stands for slow modulation, PD stands for photodiode and FP stands for Fabry–Pérot interferometer.

Fabry Pérot (FP) interferometer used for frequency calibration (free spectral range $0.0095 \, \text{cm}^{-1}$). The other beam is used as the reference (B). The whole set-up takes place in a closed box, filled with dry nitrogen at atmospheric pressure in order to minimize the absorption by ambient water vapor. Furthermore, the use of optical fibers to conduct light and the use of fused couplers instead of beam splitters is convenient to prevent further corruption by ambient H_2O over the optical path followed by the laser beam. The three signals A, B, and FP are sent to a digital oscilloscope and to a personal computer for data acquisition (10 ms per spectrum, 11 bit resolution). We use two different absorption cells for this study: a small (10 cm long) cylindrical Pyrex cell and a multiple path White type cell (A) with a path length adjustable between 1 and 10 m [8]. For broadening measurements the White cell is filled with pure water at low pressure and completed with high purity (99.9995 %) gases nitrogen and oxygen from Air Liquide—France. The pressure is measured with an uncertainty of 0.5% using two MKS baratron manometers with 10 and 1000 Torr full scale. All measurements were done at room temperature ($296 \pm 1 \, \text{K}$). We record numerous spectra for each pressure varying from 6 to 1330 mbar for the four lines under study.

2.2. Data inversion

To retrieve the coefficients of the line we usually fit a Voigt profile to the molecular transmission. The molecular transmission $T(\sigma)$ is obtained from the three recorded signals A, B and FP in two steps. First the FP signal is used to retrieve the frequency variation law by a 5° polynomial interpolation on the interferences fringes. In the second step the method used to retrieve the molecular transmission $T(\sigma)$ is from the direct absorption signals A or B using

$A = A_0 T(\sigma)$. A_0 is what would be the laser flux in the absence of absorber in the cell. A_0 is obtained from A by a $5°$ polynomial interpolation over full transmission region. The line intensity $S(T)$ is related to the molecular transmission through the Beer–Lambert law:

$$T(\sigma) = I_T(\sigma)/I_0(\sigma) = \exp[-k(s\sigma, T, p)nl],$$

where n is the density of absorbing molecules on the optical path of length l, and the absorption coefficient $k(\sigma, T, p)$ at temperature T and for a gas pressure p is modeled using the Voigt profile

$$k_V(s\sigma, T, p) = S(T)A \frac{y}{\pi} \int_{-\infty}^{+\infty} \frac{\exp(-t^2)}{y^2 + (x - t)^2} \, \mathrm{d}t$$

with

$$A = \frac{\sqrt{\ln 2}}{\gamma_{\mathrm{Dop}} \sqrt{\pi}}, y = \sqrt{\ln 2} \frac{\gamma_{\mathrm{Col}}}{\gamma_{\mathrm{Dop}}}, x = \sqrt{\ln 2} \frac{\sigma - \sigma_0}{\gamma_{\mathrm{Dop}}},$$

where $S(T)$ is the line intensity at temperature T, σ_0 is the line center wavenumber at pressure p, γ_{Dop} is the Doppler halfwidth and γ_{Col} is the collisional halfwidth:

$$\gamma_{\mathrm{Col}} = \gamma_{\mathrm{Self}} pc + \gamma_{\mathrm{Gas}} p(1 - c),$$

where γ_{Self} is the self-broadening coefficient obtained from [4], c is the concentration of H_2O and γ_{Gas} is the broadening coefficient of the studied perturbing gas (nitrogen or oxygen). The Voigt profile cannot be expressed in analytical form but may be expressed as the real part of the complex probability function $W(x,y)$ defined by

$$W(x, y) = \frac{\mathrm{i}}{\pi} \int_{-\infty}^{+\infty} \frac{\exp(-t^2)}{x + \mathrm{i}y - t} \, \mathrm{d}t$$

which can be evaluated using the Humlicek algorithm [9]. Thus the Voigt profile is defined as

$$k_V(s\sigma, T, p) = S(T)A \, \mathrm{Re}[W(x, y)].$$

The model developed by Rautian and Sobel'man [10] that take into account Dicke narrowing leads to the expression:

$$k_R(s\sigma, T, p) = S(T)A \, \mathrm{Re}\left[\frac{W(x, y + z)}{1 - \sqrt{\pi} z W(x, y + z)}\right],$$

where a, x and y have their previous meaning and $z = \sqrt{\ln 2}(\beta/\gamma_{\mathrm{Dop}})$ where β is related to the collisional narrowing coefficient β_0 by $\beta = \beta_0 p$. We check that the apparatus function of the spectrometer was negligible by recording low pressure (<0.05 mbar) spectra. In these conditions the lineshape could be fitted by a simple Gaussian curve having a Doppler width in good agreement with the theoretical value.

Fig. 2 gives an example of a spectrum recorded for the study of the $6_{6\,0} \leftarrow 6_{6\,1}$ of the $\nu_1 + \nu_3$ band of H_2O at 7185.5960 cm^{-1} diluted in N_2. The experimental spectrum, the fitted calculated spectrum described by a Rautian profile and the observed calculated residuals obtained using the Voigt profile and the Rautian model are presented. The figure demonstrates a small improvement obtained when Dicke narrowing is taken into account with Rautian model. The Rautian profile gives systematically slightly higher results of collisional widths at low pressure however the slopes of the straight lines obtained by plotting γ_{Gas} vs. p are comparable. No attempt was made to
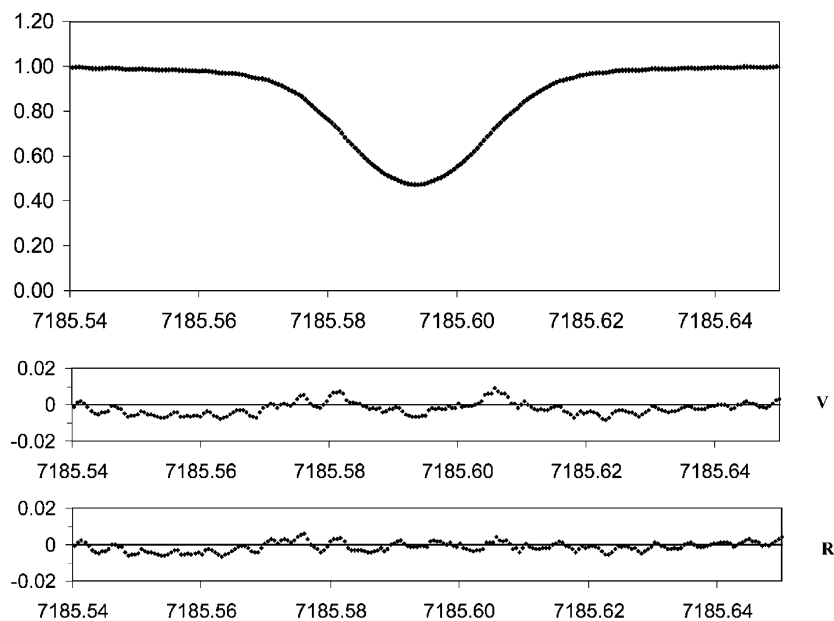
Fig. 2. Example of spectrum for the $6_{6\ 0} \leftarrow 6_{6\ 1}$ of the $v_1 + v_3$ band of H_2O at $7185.5960\,cm^{-1}$ diluted in N_2 (pressure is $44\,mbar$ and concentration is 2%). Experimental profile, fitted Rautian profile and residuals of the observed spectrum and calculated ones described by Voigt profile (V) and Rautian model (R) are presented here.

Table 2
Absolute lines intensities for H_2O at $296\,K$ and comparison with previous determinations

Line number	Intensities S ($10^{-22}\,cm^{-1}$ (molecule cm^{-2})) and differences (%)								
	S (this work)	S [5]	Diff. (%)	S [4]	Diff. (%)	S [6]	Diff. (%)	S [12]	Diff. (%)
1[a]	7.85	7.58	3.4	7.11	9.4	7.85	0.0	7.65	2.5
2	36.9	37.2	−0.8	53.0	−43.6			36.8	−0.3
3	142	143	−0.7	180	−26.8			147	−3.5
4	2.59	2.44	5.8	2.27	12.3			2.61	−0.8

[a]This line is in fact an unresolved doublet. The strength given here corresponds to the sum of the strengths of the two lines. The rotational quantum assignment given in Table 1 corresponds to the strongest transition.

obtain the value of β since two recent papers give this value for H_2O in this region: $0.025\,cm^{-1}\,atm^{-1}$ for air [6,11].

2.3. Experimental results

The intensities of the four studied lines are reported in Table 2 with the comparison with other measurements and calculations in this region. The linestrengths were measured at various temperatures as reported in [3]. The complete set of H_2O transitions lying within the tuning range of the THALES laser diode is also reported in [3]. The difference between our measurements and

the previous determinations are given in %. For absolute intensities our uncertainty is about 2%. For each line this uncertainty corresponds to one standard deviation obtained by averaging the different measurements. Our measurements are in good agreement with those of Toth [5] for the strongest lines obtained from Fourier Transform spectrometer. For lower intensities the difference remains lower than 6%. For all lines the difference with HITRAN database [4] is quite large and varies from –44% to +13%. The agreement is excellent with the value from Lepère [6] obtained by diode laser spectroscopy. For all lines the difference with the calculated Partridge data [12] is quite small demonstrating that in this region the ab initio calculations are in very good agreement with the experimental results. All the results concerning the intensities will influence strongly the H_2O retrieval in the atmosphere.

Fig. 3 presents an example of the pressure dependence of the collisional halfwidth by N_2 for the lines 1 and 4. The slope of the best fit lines represent the collisional halfwidth coefficient. For some lines the maximal pressure for the calculation of the slope was only 600 mbar due to strong adjacent lines.

Table 3 shows the experimental values for the broadening coefficients of H_2O by N_2 along with the comparison with previous determinations. For all lines our uncertainty is about 2–3%. These uncertainties are the sum of the statistical errors derived from the linear fit. For lines 1 and 3 our value corresponds to the mean value of the other experimental results. For lines 2 and 4, our value is slightly higher.

Table 4 shows the experimental values for the broadening coefficients of H_2O by O_2 along with the comparison with previous determinations. For all lines our uncertainty is about 2%. For lines 1 and 2 our value corresponds to the mean value of the other experimental results. For line 3 our value is slightly lower and slightly higher for line 4. All these experimental results are very consistent with each other. One should remark that the ratio $\gamma(N_2)/\gamma(O_2)$ is approximately equal to 1.7.
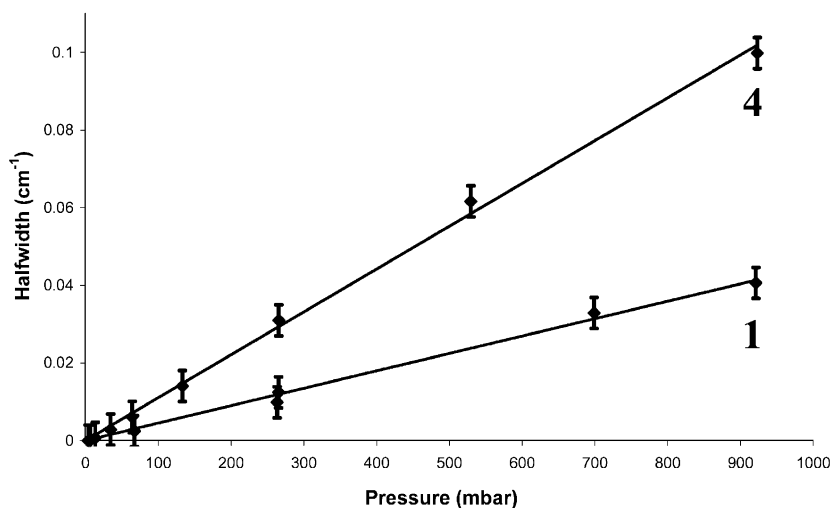

Fig. 3. Pressure dependence of the collisional halfwidth for the line 1 ($6_{6\,0} \leftarrow 6_{6\,1}$ at 7185.5960 cm^{-1}) and for the line 4 ($3_{0\,3} \leftarrow 3_{2\,2}$ at 7175.98675 cm^{-1}) of the $\nu_1 + \nu_3$ band of H_2O perturbed by N_2.

Table 3
Broadening coefficients of H_2O by N_2 and comparison with previous determinations

Line number	Broadening coefficients γ (cm^{-1} atm^{-1}) by N_2 and differences (%)								
	γ (this work)	γ [13]	Diff. (%)	γ [11]	Diff. (%)	γ [6]	Diff. (%)	γ [14]	Diff. (%)
1	0.0456	0.0429	5.9	0.0484	−6.1	0.0469	−2.9	0.0470	−3.1
2	0.1076	0.1056	1.9	0.1000	7.1				
3	0.1138	0.1076	5.4	0.1183	−4.0				
4	0.1130	0.1004	11.1						

Table 4
Broadening coefficients of H_2O by O_2 and comparison with previous determinations

Line number	Broadening coefficients γ (cm^{-1} atm^{-1}) by O_2 and differences (%)						
	γ (this work)	γ [13]	Diff. (%)	γ [11]	Diff. (%)	γ [6]	Diff. (%)
1	0.0271	0.0323	−19.2	0.0284	−4.6	0.0258	4.8
2	0.0620	0.0647	−4.4	0.0580	6.5		
3	0.0644	0.0677	−5.1	0.0694	−7.8		
4	0.0664	0.0588	11.4				

Table 5
Broadening coefficients of H_2O by air

Line number	Broadening coefficients γ (cm^{-1} atm^{-1}) by air and differences (%)								
	γ (this work)	γ [13]	Diff. (%)	γ [11]	Diff. (%)	γ [6]	Diff. (%)	γ [4]	Diff. (%)
1	0.0417	0.0407	2.4	0.0442	−6.0	0.0425	−1.9	0.0505	−21.1
2	0.0980	0.0970	1.0	0.0912	6.9			0.0980	0.0
3	0.1034	0.0992	4.1	0.1080	−4.4			0.1031	0.3
4	0.1032	0.0917	11.1					0.0919	10.9

Our data and the previous data are calculated from $\gamma(N_2) \times 0.79 + \gamma(O_2) \times 0.21$ where $\gamma(N_2)$ and $\gamma(O_2)$ are given in Tables 3 and 4. These calculations are further compared with the HITRAN database values.

To reach the scientific objectives of the SDLA spectrometer, an accuracy better than 5–10% is required in the H_2O concentration retrieval. Hence, a precise knowledge of the H_2O molecular parameters (linestrengths and air broadening coefficient) is of high importance. Table 5 shows the experimental values for the broadening coefficients of H_2O by air along with the comparison with previous determinations. Our data and the previous data are calculated from $\gamma(N_2) \times 0.79 + \gamma(O_2) \times 0.21$ where $\gamma(N_2)$ and $\gamma(O_2)$ are given in Tables 3 and 4. For lines 1 and 3 our value corresponds to the mean value of the other experimental results. For lines 2 and 4, our value is slightly higher. This trend is the same that the trend observed for $\gamma(N_2)$ because the influence of $\gamma(O_2)$ is small in this calculation. The values for lines 2 and 3 are in very good

agreement with the HITRAN database values but lines 1 and 4 show big differences up to 20% for line 1. This difference will influence the retrieval of the H_2O concentration in the atmosphere. Our experimental data will be compared in the next part with calculations based on the Robert–Bonamy formalism.

3. Theoretical calculations

The calculations are based on the complex Robert–Bonamy (CRB) theory [15]. A full description of the formalism can be found in Refs. [16–18], here only the salient features are presented. The method is complex valued so that the half-width and line shift are obtained from a single calculation. The dynamics are developed to second order in time giving curved trajectories based on the isotropic part of the intermolecular potential [15]. This has important consequences in the description of close intermolecular collisions (small impact parameters).

Within the CRB formalism the halfwidth, γ, and line shift, δ, of a ro-vibrational transition $f \leftarrow i$ are given by minus the imaginary part and the real part, respectively, of the diagonal elements of the complex relaxation matrix. In computational form the halfwidth and line shift are usually expressed in terms of the scattering matrix [19,20]:

$$(\gamma - \mathrm{i}\delta)_{f \leftarrow i} = \frac{n_2}{2\pi c} \left\langle v \times \left[1 - \mathrm{e}^{-^R S_2(f,i,J_2,v,b)} \mathrm{e}^{-\mathrm{i}\left[S_1(f,i,J_2,v,b) + S_2(f,i,J_2,v,b) \right]} \right] \right\rangle_{v,b,J_2}, \tag{1}$$

where n_2 is the number density of perturbers and $\langle \ldots \rangle_{v,b,J_2}$ represents a average over all trajectories (impact parameter b and initial relative velocity v) and initial rotational state J_2 of the collision partner. S_1 (real) and $S_2 = {}^R S_2 + \mathrm{i}^I S_2$ are the first- and second-order terms in the expansion of the scattering matrix; they depend on the rovibrational states involved and associated collision induced jumps from these levels, on the intermolecular potential and characteristics of the collision dynamics The exact forms of the S_2 and S_1 terms are given in Refs. [16–18].

The S_1 term, which makes a purely imaginary contribution, is isotropic in the absence of any vibrational dependence of the anisotropic intermolecular forces. It has the appellation of the vibrational dephasing term and arises only for transitions where there is a change in the vibrational state. The potential leading to S_1 is written in terms of the isotropic induction and London dispersion interactions. The $S_2 = {}^R S_2 + \mathrm{i}^I S_2$ term is complex valued and results from the anisotropic interactions. The potential employed in the calculations consists of the leading electrostatic components for the H_2O–X pair (the dipole and quadrupole moments of H_2O with the quadrupole moment of N_2 or O_2) and atom–atom interactions [16,21]. The latter are defined as the sum of pair-wise Lennard–Jones 6–12 interactions [22] between atoms of the radiating and the perturbing molecules. The heteronuclear Lennard–Jones parameters for the atomic pairs can be constructed from homonuclear atom–atom parameters by the "combination rules" of Hirschfelder et al. [23] or Good and Hope [24]. The atom–atom distance, r_{ij} is expressed in terms of the center of mass separation, R, via the expansion in $1/R$ of Sack [25]. Here the formulation of Neshyba and Gamache [21] expanded to eighth order is used. Finally, recall that the isotropic component of the atom–atom potential is used to define the trajectory of the collisions within the semiclassical model of Robert and Bonamy [15].

For water vapor, the reduced matrix elements are evaluated using wavefunctions determined by diagonalizing the Watson Hamiltonian [26] in a symmetric top basis for the vibrational states involved in the transition. For the ground state the Watson constants of Matsushima et al. [27] were used. For the $v_1 + v_3$ band Watson constants were not available so the Watson constants derived by Flaud and Camy-Peyret [28] for the v_3 band were used so that the wavefunctions would have proper symmetry properties. The rotational constant for N_2 is $2.0069\,cm^{-1}$ that for O_2 is $1.4377\,cm^{-1}$ [29].

Many of the molecular parameters for the H_2O–N_2 or H_2O–O_2 systems are well known and the present calculations use the best available values from the literature. The dipole and quadrupole moments of water vapor are taken from Refs. [30,31], respectively. The quadrupole moment of nitrogen is from Mulder et al. [32] that for oxygen is from Stogryn and Stogryn [33]. The numerical values are listed in Table 6. The ionization potential of water is taken to be a vibrationally independent value of 12.6 eV [34]. For nitrogen the polarizability, $17.4 \times 10^{-25}\,cm^3$, is taken from Ref. [35] and the ionization potential, 15.576 eV, from Ref. [36]. For oxygen the polarizability, $15.80 \times 10^{-25}\,cm^3$, is taken from Ref. [35] and the ionization potential, $12.063(\pm 0.001)$ eV, from Ref. [34]. In the parabolic approximation, the isotropic part of the interaction potential is taken into account in determining the distance, effective velocity, and force at closest approach [15]. To simplify the trajectory calculations, the isotropic part of the atom-atom expansion is fit to an isotropic Lennard–Jones 6–12.

The atom–atom parameters for nitrogen-broadening of water vapor have been adjusted as described in Ref. [37]. There are not enough data for oxygen-broadening of water vapor to make similar adjustments of the potential. The final adjustment of the potential parameters was made by comparing calculated line shifts to measurement. For transitions involving changes in a number of quanta in v_1 and v_3 the calculations made using the coefficients in Eq. (4) give sufficiently good agreement with the measurements (see results there after and Ref [17]). Comparing calculations for the v_2 band with the measurements of Toth [38] indicated the ab initio value of 0.03 in Eq. (4) should be changed to 0.07. Note, a non-linear least-squares optimization of the potential parameters is currently being done.

In the present calculations, the line shape parameters have been calculated without performing the averaging over the Boltzmann distribution of velocities. Only the mean thermal value $\bar{v}$ was used as has been done in most previous calculations, i.e. the mrtv approximation. This reason is that for halfwidths of H_2O at ~300 K the mrtv calculation and the velocity averaged calculation give results within a few percent of one another [39].

Table 6
Values of electrostatic moments for the water vapor, N_2, O_2

Molecule	Multipole moment	Reference
H_2O	$\gamma = 1.8549 \times 10^{-18}\,esu$	[29]
	$Q_{xx} = -0.13 \times 10^{-26}\,esu$	[31]
	$Q_{yy} = -2.5 \times 10^{-26}\,esu$	[31]
	$Q_{zz} = 2.63 \times 10^{-26}\,esu$	[31]
N_2	$Q_{zz} = -1.4 \times 10^{-26}\,esu$	[32]
O_2	$Q_{zz} = -0.4 \times 10^{-26}\,esu$	[33]

Table 7

Broadening coefficients of H_2O by N_2, O_2 and air: experimental measurements and comparison with calculations. $\gamma(air)$ is calculated from $\gamma(N_2) \times 0.79 + \gamma(O_2) \times 0.21$

Line number	Experimental and calculated broadening coefficients γ ($cm^{-1} atm^{-1}$) and differences (%)								
	γ (N_2) exp.	γ (N_2) calc.	Diff. (%)	γ (O_2) exp.	γ (O_2) calc.	Diff. (%)	γ (air) exp.	γ (air) calc.	Diff. (%)
1	0.0456	0.0426	6.6	0.0271	0.0231	14.8	0.0417	0.0385	7.7
2	0.1076	0.1102	−2.4	0.0620	0.0551	11.1	0.0980	0.0986	−0.6
3	0.1138	0.1138	0.0	0.0644	0.0576	10.6	0.1034	0.1020	1.4
4	0.1130	0.1103	2.4	0.0664	0.0561	15.5	0.1032	0.0989	4.2

The calculations were made at 296 K for the H_2O–N_2 and H_2O–O_2 systems for four rotational transitions the $\nu_1 + \nu_3$ band. A clarification is necessary here. Since the line shape parameters, especially the line shift, depend on the vibrational state it is necessary to evaluate the S_1 term for the correct vibrational states. However as described above wavefunctions for the upper state used the Watson constants of ν_3 band. This affects the S_2 term but is generally small. The experimental and calculated broadening coefficients of the 4 lines of H_2O by N_2, O_2 and air are presented in Table 7. There is a very good agreement between experimental results (uncertainty approximately 2–3%) and calculations (uncertainty approximately 5 %) for $\gamma(N_2)$. This work demonstrates the very good quality of the calculations based on the RB formalism. For H_2O–O_2 mixtures the results are not as good but this is due to not being able to adjust the potential for the H_2O–O_2 case. Finally the trend for the H_2O–Air mixture is the same as the trend for the H_2O–N_2 mixture because of the weaker influence of $\gamma(O_2)$ in the calculation $\gamma(N_2) \times 0.79 + \gamma(O_2) \times 0.21$. We obtain very good agreement between experimental values and calculated ones. All these parameters are used in the retrieval of the in situ measurements of H_2O in the atmosphere.

4. Atmospheric measurements

Fig. 4 shows an in situ vertical concentration profile yielded by the SDLA balloonborne spectrometer in the upper troposphere and lower stratosphere in 2001 for the validation of the satellite ODIN. The instrument was flown from the CNES balloon launching facility in Aire sur Adour, in southern France (43°N). More details upon the balloon operations are found in [40]. The profile is made of a few thousands of in situ measurements obtained at 1s-intervalles during ascent/descent of the gondola in the middle atmosphere. Each concentration value is obtained by applying to the in situ spectrum, a non-linear least-squares fit to the full molecular line shape in conjunction with the atmospheric P and T measurements. The laser sweeps different H_2O transitions during the flight to compensate for the decrease with altitude in the H_2O content as reported in Fig. 4.

In the dehydrated lower stratosphere, we have selected the strong $\nu_1 + \nu_3$, $(2_0\ _2) \leftarrow (3_0\ _3)$ transition at 7181.15 cm^{-1} with a line strength of $\sim 10^{-20}\ cm^{-1} mol^{-1} cm^2$. At lower altitude, the $\nu_1 + \nu_3$, $(2_1\ _2) \leftarrow (3_1\ _3)$ and $(6_6\ _0) \leftarrow (6_6\ _1)$ transitions at 7182.9 and 7185.5 cm^{-1} were chosen that feature weaker line strengths of $\sim 10^{-21}$ and $\sim 10^{-22}\ cm^{-1} molecule^{-1} cm^2$. The selection of the
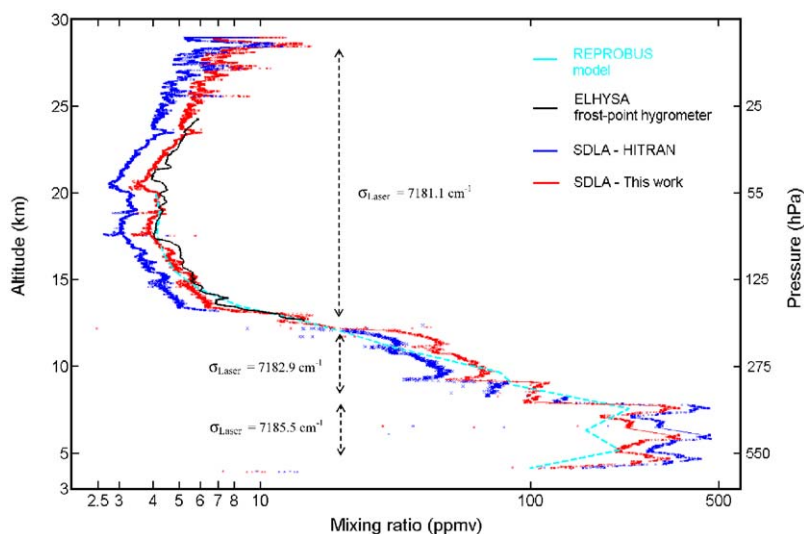
Fig. 4. A vertical in situ concentration profile of H_2O yielded by the balloonborne laser diode spectrometer SDLA in southern France on 16 October 2001. The H_2O data yielded 1 week later by the ELHYSA balloonborne frost-point hygrometer as well as the REPROBUS model predictions for the day of the flight are added on the figure. The calculation of the SDLA data was made using the HITRAN molecular parameters and the revisited molecular data set reported in this paper.

H_2O line swept over by the laser was made by observing in real-time the in situ spectra during the flight and by changing the laser operating temperature accordingly [40]. The altitude\pressure range is displayed in Fig. 4, for each selected H_2O transition. The in situ H_2O measurements yielded in the lower stratosphere by the ELHYSA balloonborne frost-point hygrometer at the same period of time as well as the predicted H_2O concentration values from the REPROBUS model are further displayed in Fig. 4. The ELHYSA frost-point hygrometer was developed 20 years ago at the Laboratoire de Météorologie Dynamique in France: for 20 years, it has been operated from aircrafts or balloons for H_2O science purposes or for satellites validation [41,42]. The ELHYSA sensor is a reference with regards to the in situ monitoring of stratospheric H_2O and its data are reported in Fig. 4 to better stress up the dramatic improvement achieved by processing the SDLA measurements with the revisited molecular parameters. REPROBUS is a three-dimensional chemical-transport model driven by the 6-h ECMWF analysis [43]. The model profile plotted in Fig. 4 is obtained after about 1 year of simulation, and was extracted in spatial and temporal coincidence with the balloon flight. Note that below the tropopause the H_2O mixing ratio in REPROBUS is forced by the ECMWF analysis of specific humidity. Using the revisited molecular parameters, a much better agreement is further observed in the tropopause between the in situ H_2O data yielded by the SDLA and the REPROBUS predictions.

In Fig. 4, the calculations were made with both the HITRAN database and the revisited molecular data. In the stratosphere, we observed a much better agreement with ELHYSA measurements and REPROBUS predictions by using the new molecular parameters. The discrepancy of ˜25% between both concentration profiles is directly related to the difference of

25% between HITRAN and this work line strengths for the $\nu_1 + \nu_3$, $(2_{0\ 2}) \leftarrow (3_{0\ 3})$ transition (Table 2).

Fig. 5 in an expanded view on the tropospheric measurements in Fig. 4. The tropospheric water vapor data yielded by a balloonborne P, T-humidity meteorological sonde launched at the same time period is also displayed to show the agreement between the large spatial structures observed in the various profiles; nevertheless, the sonde measurements can not be used for more accurate comparisons because of the variability in the H_2O content in this region of the atmosphere. The difference of -40% and $+10\%$ between HITRAN and this work in the determination of the line strength for the $\nu_1 + \nu_3$, $(2_{1\ 2}) \leftarrow (3_{1\ 3})$ and $(6_{6\ 0}) \leftarrow (6_{6\ 1})$ transitions still propagate in the vertical profiles. Around 8 km, the laser emission wavelength was changed from 7182.9 $((2_{1\ 2}) \leftarrow (3_{1\ 3}))$ to 7185.5 cm^{-1} $((6_{6\ 0}) \leftarrow (6_{6\ 1}))$: in the resulting vertical profile, we observe a much better overlapping between both altitude region using the new molecular parameters. It is a good insight for the overall coherency of the molecular data set.

Furthermore, for the $(6_{6\ 0}) \leftarrow (6_{6\ 1})$ transition at 7185.5 cm^{-1}, in addition to the 10% difference between both line strengths, a large discrepancy of 20% in the pressure-broadening coefficients was assessed between our measurement and the HITRAN database. To find out how the error propagates, a vertical concentration profile was calculated by combining our intensities and the pressure-effect coefficients extracted from the HITRAN database. The achieved profile is displayed in Fig. 5.

Figs. 6(a) and (b) display an elementary atmospheric H_2O spectrum recorded at 6.6 km by scanning of the $(6_{6\ 0}) \leftarrow (6_{6\ 1})$ transition. In Fig. 6(a), the spectrum is fitted using our molecular data. Furthermore, in the corresponding atmospheric pressure range, one could suspect a
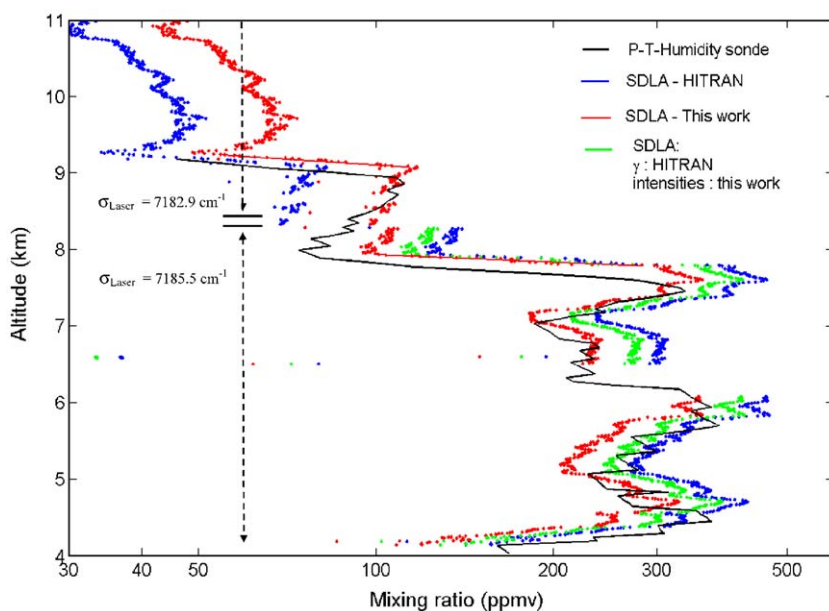

Fig. 5. An expanded view on the H_2O data in Fig. 4 obtained in the lower layers of the atmosphere. The humidity measurements recorded by a balloonborne meteorological sonde launched 1 h after the SDLA are also displayed. See text for more details.
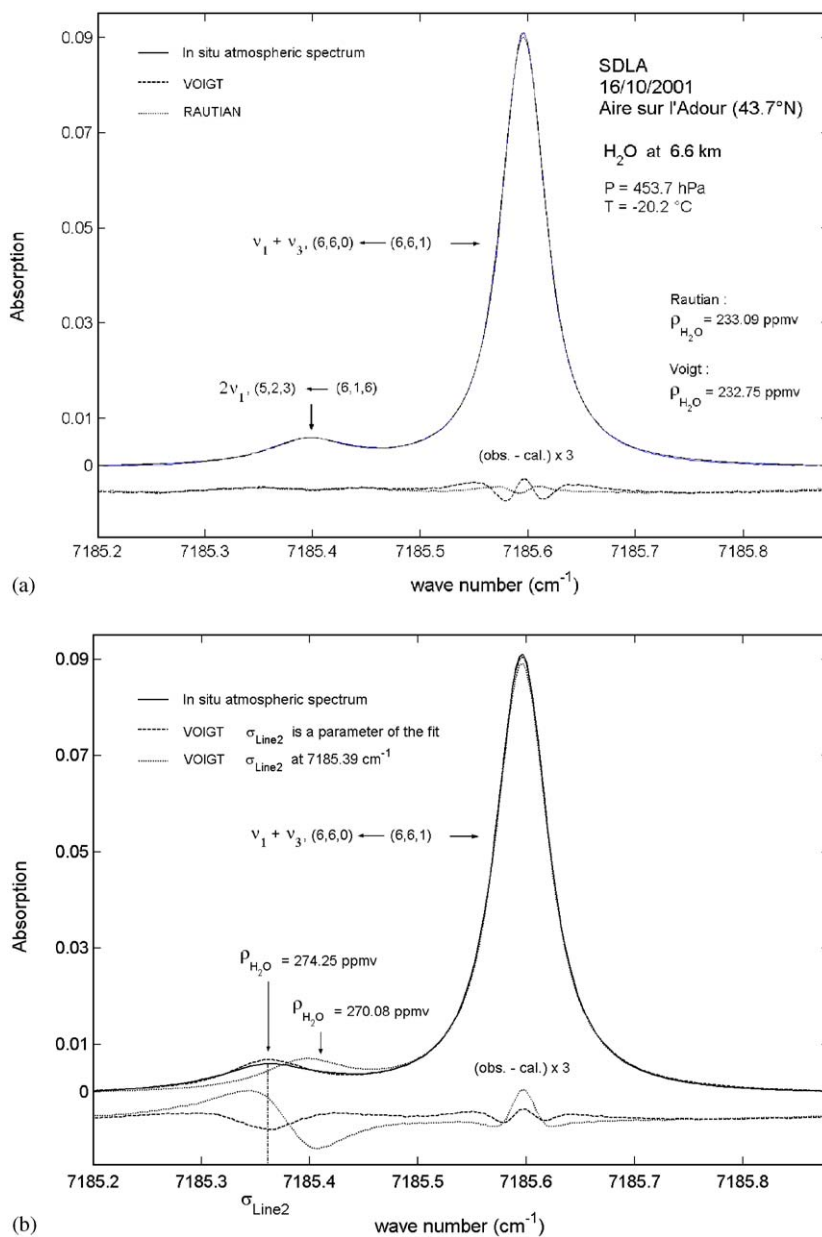
Fig. 6. (a) An in situ absorption spectrum of tropospheric H_2O recorded by the SDLA during the flight in Aire sur Adour. The measurement time is of 320 ms. To retrieve the mixing ratio, a non-linear least-squares fit is applied to the full molecular line shape in conjunction with the in situ atmospheric P and T measurements and by use of the set of molecular parameters reported in this work. A Voigt and a Rautian profile are used to model the line shape. (b) The same spectrum fitted using with the line strengths reported in this paper, but by use of the pressure-broadening coefficients extracted from the HITRAN database. To compensate for discrepancies in the line positions observed in the HITRAN database, the position of the weak $2\nu_1$, $(5_{2\ 3}) \leftarrow (6_{1\ 6})$ H_2O transition is to be released in the fit procedure.

contribution of Dicke narrowing effect to the line width; therefore, the spectrum was fitted successively using a Voigt and a Rautian profile. When fitting with a Rautian profile, the value of the pressure-broadening coefficient was slightly increased to $0.0427\,cm^{-1}\,atm^{-1}$ in agreement with the theory and the diffusion coefficient is taken to $0.025\,cm^{-1}\,atm^{-1}$ [6,11]. The fit is better using a Rautian model in terms of observed minus calculated values, as shown in Fig. 6(a). Nevertheless, in term of retrieved concentration, the difference (less than 0.001%) is not significant, given the overall measurement error. Basically, the concentration is given by the surface under the line shape which is only slightly modified here while fitting with a Rautian instead of a Voigt profile. The calculation with a Rautian model was kept further for the complete altitude range and the conclusion is the same, i.e. in terms of concentration, its effect is negligible.

In Fig. 6(b), we show the result of a fit combining our intensities and the pressure-broadening coefficients extracted from HITRAN. Using the HITRAN database, a severe line position discrepancy is observed while fitting the $2\nu_1$, $(5_{2\ 3})\leftarrow(6_{1\ 6})$ transition that neighbors the $\nu_1 + \nu_3$, $(2_{1\ 2})\leftarrow(3_{1\ 3})$ line. In a second turn, the fit was processed also by releasing the position of that transition to improve the quality of the fit. Nevertheless, the agreement is better using our molecular data regarding this weak transition (compare Fig. 6(a) and (b) near $7185.35\,cm^{-1}$). The resulting concentration values in cases (a) and (b) differ by approximately $+15\%$: hence, the error on the broadening coefficients propagate further in the overall error adding a $\sim15\%$ contribution to the $\sim10\%$ error due to the inaccuracy in the line strengths.

5. Conclusion

In this paper, a complete set of molecular parameters, intensities and pressure-broadening coefficients, was determined theoretically and experimentally near $1.39\,\mu m$ for several H_2O transitions of interest for the in situ laser sensing of the middle atmosphere. The achieved ab initio and laboratory measurements were thoroughly compared to previous determinations and existing molecular databases. A dramatic improvement in the accuracy of the line strengths and pressure coefficients was achieved for the selected molecular transition of the order of ten percent, with a direct impact on the quality of H_2O concentration values yielded by our balloon borne laser hygrometer in the lower stratosphere and upper troposphere.

References

[1] Durry G, Mégie G. Atmospheric CH_4 and H_2O monitoring with near-infrared InGaAs laser diodes by the SDLA, a balloonborne spectrometer for tropospheric and stratospheric in situ measurements. Appl Opt 1999;38:7342–54.

[2] Durry G, Mégie G. In situ measurements of H_2O from a stratospheric balloon by diode laser direct-differential absorption spectroscopy at 1.39 μm. Appl Opt 2000;39:5601–8.

[3] Parvitte B, Zéninari V, Pouchet I, Durry G. Diode laser spectroscopy of H_2O in the 7165–7185 cm^{-1} range for atmospheric application. JQSRT 2002;75:493–507.

[4] Rothman LS, Barbe A, Chris Benner D, Brown LR, Camy-Peyret C, Carleer MR, Chance K, Clerbaux C, Dana V, Devi VM, Fayt A, Flaud J-M, Gamache RR, Goldman A, Jacquemart D, Jucks KW, Lafferty WJ, Mandin J-Y, Massie ST, Nemtchinov V, Newnham DA, Perrin A, Rinsland CP, Schroeder J, Smith KM, Smith MAH, Tang K, Toth RA, Vander Auwera J, Varanasi P, Yoshino K. The HITRAN molecular spectroscopic database: edition of 2000 including updates through 2001. JQSRT 2003;82:5–44.

[5] Toth RA. Extensive measurements of H_2O line frequencies and strengths: 5750 to 7965 cm^{-1}. Appl Opt 1994;33:4851–67.

[6] Lepère M, Henry A, Valentin A, Camy-Peyret C. Diode laser spectroscopy: Line profiles of H_2O in the region of 1.39 μm. J Mol Spectrosc 2001;208:25–31.

[7] Camy-Peyret C, Flaud JM, Maillard JP, Guelachvili G. Higher ro-vibrational levels of H_2O deduced from high resolution oxygen-hydrogen flame spectra between 6200 and 9100 cm^{-1}. Mol Phys 1977;33:1641.

[8] Courtois D, Delahaigue A, Thiébeaux C, Le Corre H, Mouanda J-C. Adjustable-temperature and multiple-path optical cell for ozone spectroscopy. J Phys E: Sci Instrum 1988;21:863–5.

[9] Humlicek J. Optimized computation of the Voigt and complex probability functions. JQSRT 1982;27:437–44.

[10] Rautian SG, Sobel'man IC. Sov. Phys Usp 1967;9:701–16.

[11] Moretti L, Sasso A, Gianfrani L, Ciurylo R. Collisional-broadened and Dicke-narrowed lineshapes of $H_2^{16}O$ and $H_2^{18}O$ transitions at 1.39 μm. J Mol Spectrosc 2001;205:20–7.

[12] Partridge H, Schwenke DW. The determination of an accurate isotope dependent potential energy surface for water from extensive ab initio calculations and experimental data. J Chem Phys 1997;106:4618–35.

[13] Delaye C, Hartmann J-M, Taine J. Calculated tabulations of H_2O line broadening by H_2O, N_2, O_2, and CO_2 at high temperature. Appl Opt 1989;28:5080–7.

[14] Nagali V, Chou SI, Baer DS, Hanson RK. Diode laser measurements of temperature-dependent half-widths of H_2O transitions in the 1.4 μm. JQSRT 1997;57:795–809.

[15] Robert D, Bonamy J. Short range force effects in semiclassical molecular line broadening calculations. J Phys 1979;40:923–43.

[16] Gamache RR, Lynch R, Neshyba SP. New developments in the theory of pressure-broadening and pressure-shifting of spectral lines of H_2O: the complex Robert–Bonamy formalism. JQSRT 1998;59:319–35.

[17] Lynch R, Gamache RR, Neshyba SP. N_2 and O_2 induced halfwidths and line shifts of water vapor transitions in the (301)←(000) and (221)←(000) bands. JQSRT 1998;59:595–613.

[18] Lynch R. Ph.D. dissertation, Physics Department, University of Massachusetts Lowell, June 1995.

[19] Baranger M. General impact theory of pressure broadening. Phys Rev 1958;112:855–65.

[20] Ben-Reuven A. Spectral line shapes in gases in the binary-collision approximation. In: Prigogine I, Rice SA, editors. Advances in chemical physics, vol. 20. New York: Academic Press; 1975. p. 235.

[21] Neshyba SP, Gamache RR. Improved line broadening coefficients for asymmetric rotor molecules: application to ozone perturbed by nitrogen. JQSRT 1993;50:443–53.

[22] Lennard-Jones JE. On the determination of molecular fields-II: From the equation of state of a gas. Proc Roy Soc 1924;A106:463–77.

[23] Hirschfelder JO, Curtiss CF, Bird RB. Molecular theory of gases and liquids. New York: Wiley; 1964.

[24] Good RJ, Hope CJ. Test of combining rules for intermolecular distances, potential function constants from second virial coefficients. J Chem Phys 1971;55:111–6.

[25] Sack RA. Two-center expansion for the powers of the distance between two points. J Math Phys 1964;5:260–8.

[26] Watson JKG. Determination of centrifugal distortion coefficients of asymmetric-top molecules. J Chem Phys 1967;46:1935–49.

[27] Matsushima F, Odashima H, Iwaskai T, Tsunekawa S. Frequency measurement of pure rotational transitions of H_2O from 0.5 to 5 THz. J Mol Struct 1995;352–353:371–8.

[28] Flaud JM, Camy-Peyret C. Watson Hamiltonian constants for the first vibrational levels of H_2O. Private communication, 1997.

[29] Huber KP, Herzberg G. Molecular spectra and molecular structure constants of diatomic molecules. New York: Van Nostrand; 1979.

[30] Shostak SL, Muenter JS. The dipole moment of water. II. Analysis of the vibrational dependence of the dipole moment in terms of a dipole moment function. J Chem Phys 1991;94:5883–90.

[31] Flygare WH, Benson RC. Molecular Zeeman effect in diamagnetic molecules and the determination of molecular magnetic moments (g values), magnetic susceptibilities, and molecular quadrupole moments. Mol Phys 1971;20:225–50.

[32] Mulder F, Van Dijk G, Van der Avoird A. Multipole moments, polarizabilities, and anisotropic long range interaction coefficients for nitrogen. Mol Phys 1980;39:407–25.

[33] Stogryn DE, Stogryn AP. Mol Phys 1966;11:371–93.

[34] Lide DR, editor. CRC handbook of physics and chemistry, 77th ed. Clevland, OH: The Chemical Rubber Company; 1996.

[35] Bogaard MP, Orr BJ. MPT international review of science, physical chemistry. In: Buckingham AD, editor. Molecular structure and properties, vol. 2. London: Butterworths; 1975 Chapter 5.

[36] Lofthus A. The molecular spectrum of nitrogen. Department of Physics, University of Oslo, Blindern, Norway, Spectroscopic Report No. 2, 1960.

[37] Gamache RR, Hartmann JM. Collisional parameters of H_2O lines: effects of vibration. JQSRT 2004;83:119–47.

[38] Toth RA. Air- and N_2-broadening parameters of water vapor: 604 to 2271 cm^{-1}. J Mol Spectrosc 2000;201:218–43.

[39] Gamache RR, Rosenmann L. The effects of velocity averaging in broadening coefficient calculations. J Mol Spectrosc 1994;164:489–99.

[40] Durry G, Pouchet I. A near-infrared diode laser spectrometer for the in situ measurements of CH_4 and H_2O from stratospheric balloons. J Atmos Ocean Technol 2001;18:1485–94.

[41] Ovarlez J. Stratospheric water vapor measurement in the tropical zone by means of a frost-point hygrometer on board long-duration balloons. J Geophys Res 1991;96:15541–5.

[42] Ovarlez J, Ovarlez H. Stratospheric water vapor content evolution during EASOE. Geophys Res Lett 1994;21:1235–8.

[43] Lefèvre F, Figarol F, Carslaw KS, Peter T. The 1997 Arctic ozone depletion quantified from three-dimensional model simulations. Geophys Res Lett 1998;25:2425–8.